



OPEN ACCESS

EDITED BY

Armstrong-Altrin John S.,
National Autonomous University of Mexico,
Mexico

REVIEWED BY

Benjun Ma,
Harbin Engineering University, China
Mayla Ramos,
Instituto Potosino de Investigación Científica
y Tecnológica (IPICYT), Mexico

*CORRESPONDENCE

Ya Gao

✉ gaoy355@mail.sysu.edu.cn

RECEIVED 28 October 2024

ACCEPTED 24 December 2024

PUBLISHED 28 January 2025

CITATION

Chen B, Xu L, Liu B, Zhang L, Xiao D, Gao Y,
Wu F, Yang X, Zou Y, Ma Y and Zhang Y
(2025) Characterizing a complex buildup in
the Pearl River Mouth Basin of the northern
South China Sea: an interplay of carbonates
and igneous rocks.
Front. Mar. Sci. 11:1518292.
doi: 10.3389/fmars.2024.1518292

COPYRIGHT

© 2025 Chen, Xu, Liu, Zhang, Xiao, Gao, Wu,
Yang, Zou, Ma and Zhang. This is an open-
access article distributed under the terms of
the [Creative Commons Attribution License
\(CC BY\)](https://creativecommons.org/licenses/by/4.0/). The use, distribution or reproduction
in other forums is permitted, provided the
original author(s) and the copyright owner(s)
are credited and that the original publication
in this journal is cited, in accordance with
accepted academic practice. No use,
distribution or reproduction is permitted
which does not comply with these terms.

Characterizing a complex buildup in the Pearl River Mouth Basin of the northern South China Sea: an interplay of carbonates and igneous rocks

Beichen Chen¹, Leyi Xu¹, Baojun Liu¹, Lili Zhang¹, Dong Xiao¹,
Ya Gao^{2,3*}, Feng Wu⁴, Xueqi Yang¹, Yaming Zou¹,
Yongkun Ma¹ and Yinglin Zhang¹

¹Research Institute, Shenzhen Branch of China National Offshore Oil Corporation Ltd., Shenzhen, China, ²School of Marine Sciences, Sun Yat-sen University, Zhuhai, China, ³Hubei Key Laboratory of Marine Geological Resources, China University of Geosciences (CUG), Wuhan, China, ⁴College of Oceanography, Hohai University, Nanjing, China

Volcanic mounds and carbonate buildups share similar geometries, making their differentiation in seismic data a significant challenge. This challenge is further compounded in complex buildups composed of both multi-stage developed igneous rocks and biogenic carbonates. To address this gap, this study investigates a mixed carbonate-igneous buildup at the central of the Baiyun Sag in the northern South China Sea. By analyzing the lithofacies of the carbonates and igneous rocks, the morphological features and spatial distribution patterns corresponding to these sedimentary and volcanic facies were identified. Well-to-seismic calibration was used to delineate the stratigraphic units, and typical seismic profiles of the buildup were analyzed. Eight distinct seismic facies were identified for carbonates and igneous rocks. The evolution of the buildup is divided into three stages: (1) volcanic eruptions and carbonates development, (2) overflowing magma and reef shoal deposits, and (3) reef-bank deposition accompanied by igneous intrusion. We propose that volcanic rocks can be distinguished from carbonates by the temporal and spatial coupling of typical features: (a) surface volcanic rocks and subsurface intrusive bodies are inseparable, with igneous rocks identifiable through faults and volcanic conduits; (b) carbonates typically display symmetrical structures on both sides of the highland and exhibit better stratification away from igneous activity; (c) carbonates generally show a convex clinoform and steep slope at the platform margin, while volcanic mounds exhibit concave gentle slopes. Furthermore, the analysis of high-quality reservoir development within the complex buildups is instrumental for advancing oil and gas exploration in volcanic seamounts and carbonate buildups.

KEYWORDS

carbonate platform, volcanic mound, seismic facies, platform evolution, the baiyun sag

1 Introduction

Carbonate platforms have long been a focal point in sedimentology and a key target for hydrocarbon exploration. Numerous case studies have documented the development of carbonates formations within petroleum basins (Isern et al., 2004; Bachtel et al., 2010; Tian et al., 2015; Reolid et al., 2020; Ting et al., 2021; Qiao et al., 2024). Their evolution is influenced by a variety of factors, including tectonic activity, changes in relative sea level, and variations in temperature, light, and nutrient variations (Tomás et al., 2008; Betzler et al., 2013; Shao et al., 2017; Courgeon et al., 2017; Coletti et al., 2019; Luo et al., 2023). These factors impact not only the rate of carbonate stratigraphy development but also the structural patterns and lithological facies (Atasoy et al., 2018; Dimou et al., 2024; Su et al., 2024).

As the other kind of submarine highs in marine environments, volcanic mounds that often resemble isolated seamounts are also commonly found in oil- and gas-prone basins (Svensen et al., 2004; Silva et al., 2024). Carbonates developed on volcanic pedestal platforms also have been widely documented (Bosence, 2005; Courgeon et al., 2016; Courgeon et al., 2017; Counts et al., 2018; Tucker et al., 2020). In practical research, seismic facies characteristics of volcanic mounds and isolated carbonate buildups often appear similar, making differentiation based solely on seismic data challenging (Burgess et al., 2013; Ma et al., 2018a). However, distinguishing between the two is critical, as volcanic mounds typically have different porosity and permeability compared to carbonate platforms, which significantly influences hydrocarbon reservoir evaluation (Greenlee and Lehmann, 1993).

This study focuses on a complex buildup composed of both carbonates and igneous rocks in the Baiyun Sag of the Pearl River Mouth Basin, dating from the late Oligocene to early Miocene. While Well A has provided some insights into the local lithology of this buildup, the lack of a comprehensive analysis of its internal structure has limited the oil and gas exploration potential and reduced confidence in the exploration of similar seamounts or mound-type targets. Therefore, this study employs recently reprocessed three-dimensional (3D) geophysical data to offer a detailed seismic analysis and an evolutionary model of the complex buildup, with aims of: (1) discriminating volcanic rocks from carbonates in seismic profiles; (2) providing a valuable analogue for understanding the structure and composition of volcanic rocks associated with carbonate platforms, and (3) predicting the distribution of oil and gas reservoirs in comparable mixed carbonate-igneous buildup.

2 Geological background

The Baiyun Sag located in the northern South China Sea occupies an area of 2.1×10^4 km² (Figures 1A, B), with sedimentary thickness exceeding 11 km. Its boundary is defined by the Panyu Low Salient in the north, the Dongsha Rise in the east, and the Yunkai Low Salient in the west. The investigated buildup, between 115°–116°E, and 19°–20°N at the central region of the

Baiyun Sag (Figure 1C) is the necking zone of the Pearl River Mouth Basin, where the crust has experienced significant stretching and thinning (Mohn et al., 2012; Ren et al., 2015).

During the late Oligocene and early Miocene, multiple episodes of volcanic activities (Zhao et al., 2016; Deng et al., 2019; Sun Q. et al., 2014) caused numerous shallow magmatic intrusions. The intense volcanic activity associated with the activities of the deep original mantle beneath the Baiyun Sag (Zhou et al., 2009; Li et al., 2015; Zeng et al., 2019; Zhou et al., 2020) led to the formation of the investigated buildup above the central diapir zone. The development of the complex buildup occurred within a shallow marine shelf environment while the shelf break was located near the Panyu Low Salient (Tian et al., 2019; Zhang et al., 2019). Regional stratigraphic studies and paleontological dating indicate that the complex buildup ceased growing after 23.8 Ma. After that, the study area transitioned to a semi-deep-sea environment, marked by the development of thick mudstones above the buildup.

During the Cenozoic, the Pearl River Mouth Basin underwent six major tectonic movements that significantly influenced the evolution of structural sedimentation (Feng and Zheng, 1982; Pinglu and Chuntao, 1994; Ma et al., 2015; Ma et al., 2018b; Zhou et al., 2009; Sun Z et al., 2014), with varying degrees of impact on the Baiyun Sag (Figure 2A). The Shenhu Movement, occurring approximately 66 Ma, is characterized by a regional unconformity (Tg), marking the basement of the Cenozoic basin. The Zhuqiong Movement took place around 47.8 Ma, appearing as a regional unconformity (T90). A second phase of the Zhuqiong Movement occurred around 38 Ma, forming another regional unconformity (T80). The South China Sea Movement occurred around 33.9 Ma, identified by a regional unconformity (T70). The Baiyun Movement, occurring around 23.03 Ma, is represented by a structural unconformity (T60). The Dongsha Movement, dated to about 11.62 Ma, is marked by a regional unconformity (T30) in the seismic data.

3 Materials and methods

3.1 Borehole data

The drilling data for this study were obtained from Well A. Lithological descriptions of the late Oligocene Zhuhai Formation were calibrated with well-log responses, including gamma-ray (GR), bulk density (RHOB), and sonic velocity (DTCO). The complex buildup (Figure 2B), located at depths between 4069.2 m and 4846.75 m, belongs to the Zhuhai Formation and is divided into three sedimentary units. Unit 4 of the Zhuhai Formation, situated beneath the complex buildup, is composed of a mixed sedimentary sequence of tuffaceous sandstone and calcareous sandstone.

A total of twenty-seven core samples (Table 1) were described and identified, with corresponding porosity and permeability data provided. Carbonates samples were obtained via sidewall coring, which generally exhibited good porosity and permeability. In contrast, the igneous rock samples collected showed almost no porosity or permeability. Rock samples from depths below 4846.75

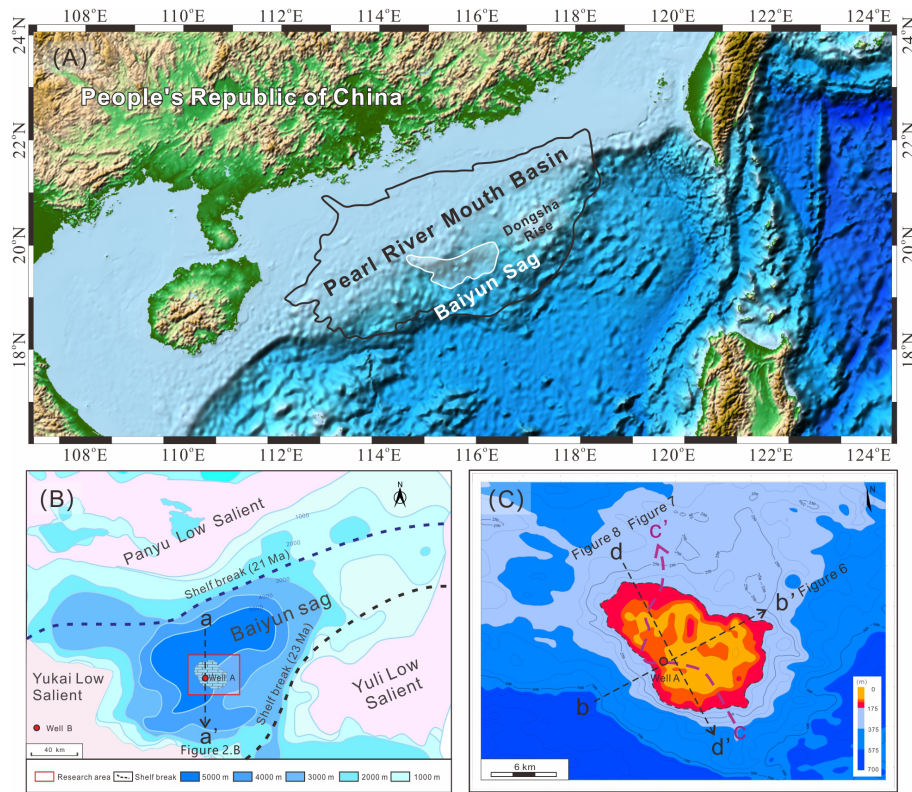


FIGURE 1

Regional geological map: (A) Location of the Pearl River Mouth Basin; (B) Sediment thickness map of Baiyun Depression. The map displays varying sedimentary thicknesses from the Wenchang Formation to the Enping Formation, with the thickest deposits occurring in the central part of the Baiyun Sag. The location of the shelf break of the Zhuhai (23 Ma) and Zhujiang (21 Ma) Formation is indicated by the dotted line in the image. (C) Morphological features of the top of the complex buildup. The picture shows the thickness map obtained by subtracting the top layer of the complex buildup from the 23.8 Ma strata.

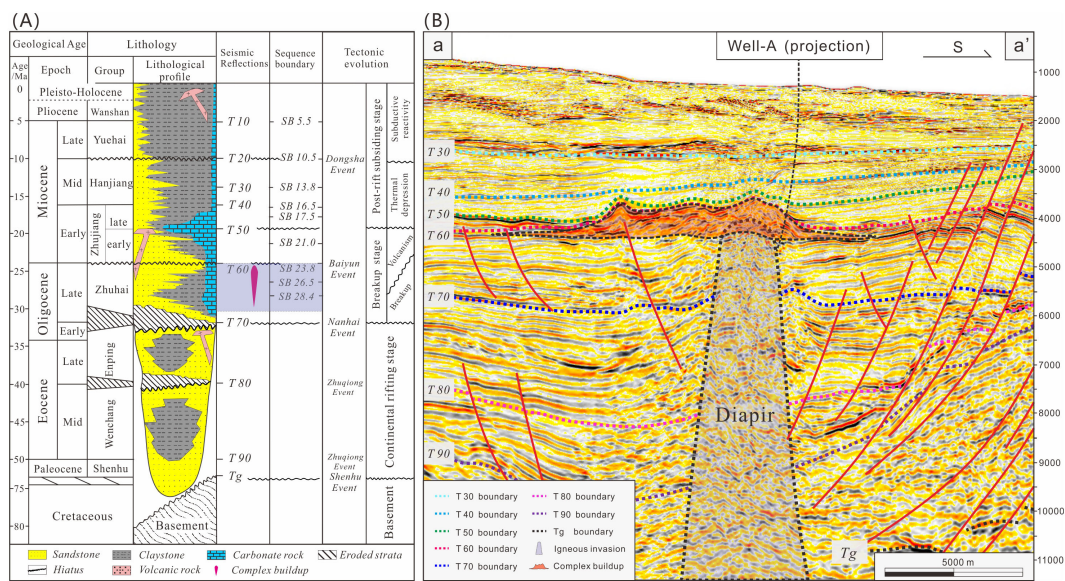


FIGURE 2

Regional comprehensive column histogram and seismic profile of stratigraphic framework: (A) Schematic stratigraphic histogram of Pearl River Mouth Basin mainly modified from Sun Z et al. (2014), Zhao et al. (2016), and Ma et al. (2018a). (B) The central diapir zone and complex buildup of Baiyun Sag. The complex buildup developed during the Zhuhai Formation and ceased before 23.8 Ma.

TABLE 1 Depth, porosity, permeability, rock type and lithofacies of rock samples.

Sample	Depth (m)	Porosity (%)	Permeability (md)	Rock type	Lithofacies
1	4088.5	12.3	0.288	Carbonates	Rudstone
2	4093.5	18.6	1.05	Carbonates	Rudstone
3	4099.6	17.4	1.14	Carbonates	Grainstone
4	4104.5	19.0	1.12	Carbonates	Grainstone
5	4107.3	/	/	Carbonates	Grainstone
6	4140.0	15.1	0.482	Carbonates	Grainstone
7	4166.5	/	/	Igneous rock	Basalt
8	4228.5	/	/	Igneous rock	Basalt
9	4254.0	/	/	Carbonates	Packstone
10	4272.5	/	/	Igneous rock	Hyaloclastite
11	4329.0	17.4	1.94	Carbonates	Grainstone
12	4334.5	7.4	0.007	Carbonates	Packstone
13	4337.0	4.2	0.002	Carbonates	Packstone
14	4356.5	6.2	0.004	Carbonates	Packstone
15	4468.5	9.2	/	Carbonates	Floatstone
16	4573.0	/	/	Carbonates	Wackestone
17	4594.5	1.1	/	Igneous rock	Diabase
18	4674.5	/	/	Carbonates	Dolomitic Limestone
19	4747.5	3.5	/	Igneous rock	Basalt
20	4753.0	3.1	/	Igneous rock	Diabase
21	4902.0	/	/	Mixed deposits	Tuff/Claystone
22	4966.9	/	/	Mixed deposits	Sandstone
23	4983.8	/	/	Mixed deposits	Tuffaceous sandstone
24	5055.3	/	/	Mixed deposits	Tuffaceous sandstone
25	5093.3	/	/	Mixed deposits	Tuffaceous sandstone
26	5143.8	/	/	Mixed deposits	Tuffaceous sandstone
27	5166	/	/	Mixed deposits	Hyaloclastite

m were collected using gunpowder coring, and their porosity and permeability are not considered relevant for this study.

3.2 Seismic data

The original 3D seismic survey was acquired in 2006 by Danwen Energy China, Ltd. In 2022, China National Offshore Oil Corporation (CNOOC) re-acquired PSTM/PSDM data from the central diapir zone (Figure 1C) in the Baiyun Sag. This re-acquisition utilized long cables (8100 m), deep source placement (12 m), increased source capacity (4365 cuin), and an optimized acquisition direction. In 2023, CNOOC processed the seismic data to generate secondary 3D PSTM/PSDM datasets. The signal-to-noise ratio of the seismic data was significantly improved, with better attenuation of multiple wave

types, resulting in clearer geological boundaries. In this study, the 2023 secondary 3D PSTM data were used for well-to-seismic calibration, while seismic interpretation and stratigraphic division were based on the PSDM data.

3.3 Facies description

Lithofacies descriptions follow the classification schemes of Dunham (1962) and Klován and Embry (1972). The original sedimentary environment of carbonates is analyzed based on the structural components and growth patterns of carbonate fabrics (Insalaco, 1998; Riding, 2002). Mixed sediments are classified as carbonate-siliciclastic deposits if they contain more than 10% of each of the two antithetic components (Chiarella and Longhitano,

2012). Seismic sequence stratigraphy is interpreted according to the methodology proposed by Van Wagoner et al. (1988). The spatial distribution of carbonates and volcanic facies is described by comparing and identifying the internal configurations and external geometries of seismic profiles. The integration of lithofacies identification and seismic facies characterization allows for the development of an evolutionary model, illustrating the depositional stages of the buildup.

4 Results and interpretation

4.1 lithological facies analysis

4.1.1 Carbonates

The lithological column for Well A provides a detailed overview of the typical carbonate facies present (Figure 3). Thin-section analysis is used to describe and interpret these lithofacies, aiding in the reconstruction of the sedimentary evolution of this complex buildup. The carbonate deposits exhibit three distinct stages, each characterized by different sedimentary features.

Carbonate depositional unit 3, located between drilling depths of 4479.25 and 4724.00 m, corresponds to a relatively deep-water environment. Sample 3 I (Figure 3I), taken from 4674.5 m, consists

of micrite limestone with notable recrystallization, suggesting deposition on a carbonate platform in deeper waters. Sample 3 H (Figure 3H), at 4573 m, is a wackestone containing red algae particles, interpreted as having formed in an open platform environment with low hydrodynamic conditions. Sample 3 G (Figure 3G), from 4468.5 m, is a floatstone with larger bioclastic particles, including suspected coral fragments and some signs of dolomitization, indicating allochthonous transport. The matrix is composed of a high proportion of lime-mudstone, abundant planktonic foraminifera and small bioclasts, pointing to lagoonal deposition in a low-energy environment.

Unit 2 of the carbonates, extending from 4321.60 to 4479.25 m, represents a bioclastic shoal developed in a wave-dominated zone. Sample 3 F (Figure 3F) at 4356.5 m is a packstone with bioclastic particles, including benthic foraminifera, red algae, echinoderms, and mollusks. The matrix is rich in lime mudstone. Sample 3 E (Figure 3E) from at 4337 m, is also a packstone with abundant bioclasts, indicating deposition in a shallow, high-energy environment with strong wave action. Sample 3 D (Figure 3D) at 4329 m, consists of grainstone with highly fragmented bioclasts and numerous visible pores. Unit 2 is predominantly composed of bioclastic limestone, reflecting a high-energy depositional environment.

Unit 1 of the carbonates, between 4069.2 and 4321.60 m, is characterized by interbedded sheet-like effusive rocks and biogenic

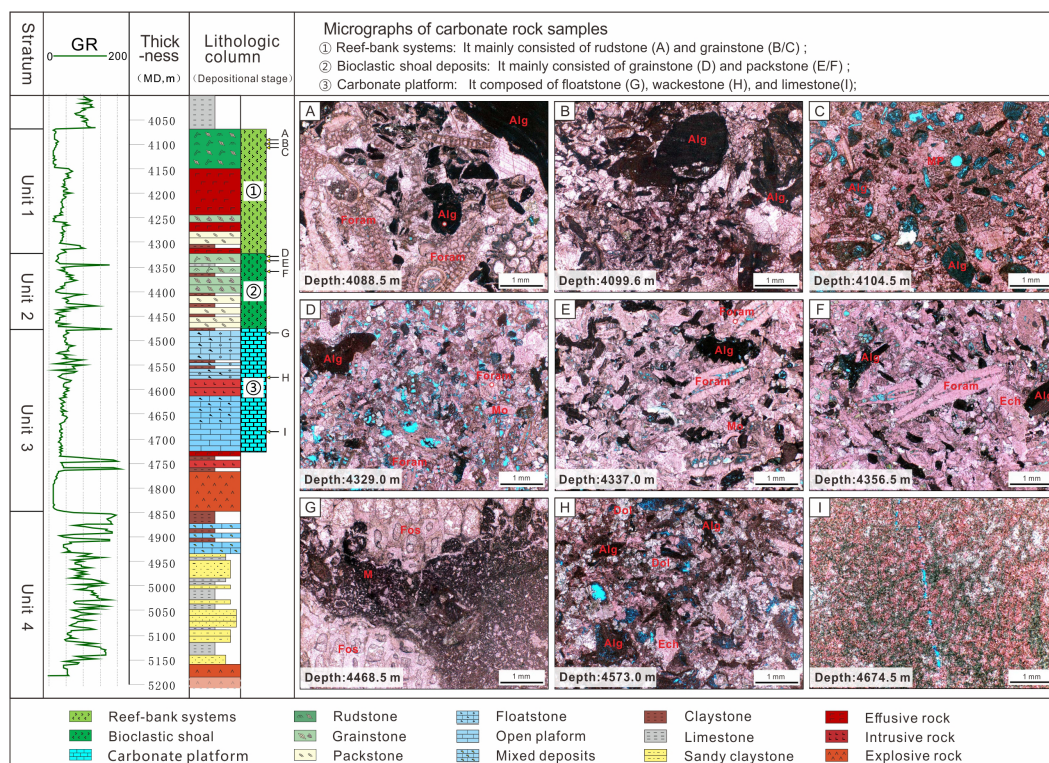


FIGURE 3

Description and Interpretation of Carbonates: (A) Rudstone: Biogenic limestone composed of benthic foraminifera (Foram) and red algae (Alg), indicating deposition in shallow water with strong hydrodynamic conditions; (B) Grainstone: Red algae particles-rich reef limestone with sparry cement; (C) Grainstone: Bioclastic limestone with abundant red algae and echinoderm (Ech) debris, featuring moldic (MP) pores; (D) Grainstone: Composed of red algae, foraminifera, and mollusks (Mo); (E) Packstone: Skeletal grains consist of foraminifera, red algae, and echinoderm; (F) Packstone: Skeletal grains composed of foraminifera, red algae, and echinoderms; (G) Floatstone: Contains suspected coral debris and planktonic foraminifera; (H) Wackestone: Small red algae grains remain intact; (I) Micritic Limestone: micrite limestone with notable recrystallization.

limestone. Sample 3 C (Figure 3C), located at 4104.5 m, is a grainstone with bioclasts including red algae, mollusks, and echinoderms. The thin sections reveal abundant moldic and intraparticle pores, though these are poorly interconnected. Sample 3 B (Figure 3B) at 4099.6 m, is a packstone with a high content of sparry cement, with bioclasts primarily consisting of red algae. Sample 3 A (Figure 3A) at 4088.5 m, is a rudstone with high sparry cement content, containing large benthic foraminifera, red algae, along with echinoderms and mollusks. Unit 1 is primarily composed of biogenic limestone, with coral fragments observed in drilling cuttings, interpreted as part of a reef-bank system deposit.

4.1.2 Volcanic rock

Igneous rocks observed in thin sections can be classified into three types of volcanic facies (Figure 4): effusive, intrusive, and extrusive rock. Effusive facies represents magma that has erupted from a volcano, forming volcanic flows. Intrusive facies are associated with shallow intrusions, such as dikes or stocks, which are formed by the cooling and solidification of magma within ascending channels. Extrusive facies indicates volcanic eruptions, where magma is expelled explosively to form pyroclastics and tuff layers. These tuff deposits generated by volcanic eruptions are interbedded with sandstones, reflecting a mixed sedimentary environment around the volcanic edifice.

In the early stage of Unit 4, core samples indicate that igneous rocks formed from underwater explosive eruptions. Sample 4 I (Figure 4I), located at 5166 m, consists of hyaloclastic rocks (Wright, 2001) that were formed during volcanic eruptions, and likely underwent significant alteration. These rocks accumulated near the volcanic crater and contributed to the development of a volcanic edifice. Tuffaceous sandstone and claystone (Figures 4G, H) exhibit mixed sedimentation from volcanic tuff and delta-front sands, indicating active volcanic activity during that period.

During the early stage of Unit 3, continued volcanic activity led to the formation of shallow intrusive and effusive rocks. Sample 4 F (Figure 4F) at 4753 m is primarily composed of plagioclase and pyroxene, with local Fe-calcite filling fractures, suggesting a shallow intrusive origin. These rocks are formed by the condensation of magma as it ascends through the strata. Sample 4 D (Figure 4D), located at 4594.5 m, exhibits a diabase texture, with plagioclase as the dominant mineral, followed by pyroxene. This sample, which lacks visible porosity, represents a shallow intrusive side vent or sill. The formation of volcanic edifices created topographic highs, providing a hardground structure that promoted the substantial development of carbonate deposits.

Effusive facies are extensively developed in Unit 1. Sample 4 C (Figure 4C), located at 4272.5 m, consists of hyaloclastic rocks, typical of products from underwater volcanic eruptions. These

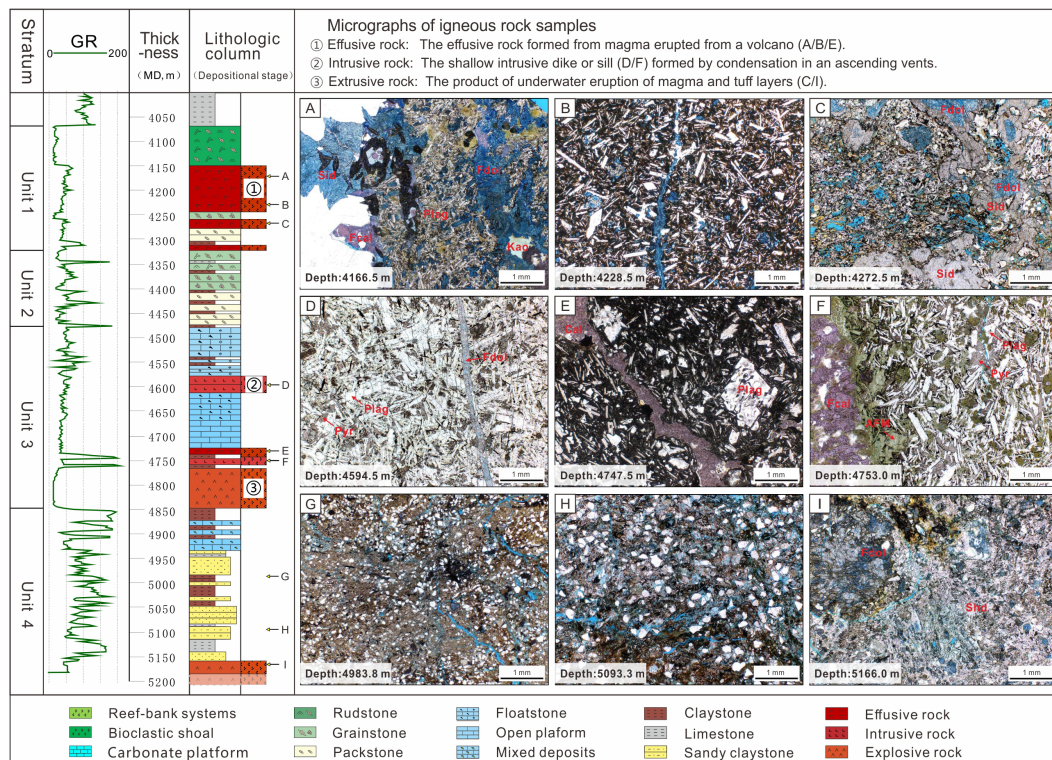


FIGURE 4 Description and interpretation of igneous rocks. (A) Basalt: associated with shallow volcanic pipes or extrusive facies; (B) Pillow basalt: formed at volcanic side vents, typically exhibiting a short overflow range and being distributed near the volcanic crater.; (C) Hyaloclastite: Formed by underwater volcanic eruptions, accumulate near the volcanic crater; (D) Diabase: shallow intrusive dyke or sill, condensed in the shallow stratum; (E) Basalt, effusive facies, exhibits a short overflow range and is located around the crater.; (F) Diabase:volcanic vent, shallow intrusive dyke or sill condenses in an ascending magma channel; (G, H) Tuff: mixed deposit consisting of pyroclastic tuff and sandstone debris. (I) Hyaloclastite: basaltic magma erupts underwater, forming pyroclastic mounds near the volcanic eruption.

rocks likely accumulated near the volcanic crater. Sample 4 B (Figure 4B), located at 4228.5 m, shows a porphyritic structure with plagioclase phenocrysts, likely representing pillow basalt formed at volcanic side vents. Sample 4 A (Figure 4A), located at 4166.5 m, is interpreted as heavily altered basalt, with plagioclase as the dominant mineral, partially replaced by chert and microcrystalline quartz. Notably, Fe-dolomite (stained dark blue) fills fractures and pores.

4.2 Well-to-seismic calibration

Core samples from carbonates and volcanic rock facies were calibrated with well-log responses to analyze the vertical variations in lithological compositions (Figure 5). Notable changes in the gamma-ray (GR) response indicate sudden significant lithological transitions. By performing a comprehensive analysis of the GR, DTCO, and RHOB curves, as well as detailed drilling data and synthetic records, a well-to-seismic calibration was conducted. This process identified five key horizons (H1-H5) and three lithological boundaries (B1-B3) within the Zhujiang Formation.

H1, calibrated at the trough, represents the interface between high-porosity limestone and the overlying dense lime-mudstone. B1 corresponds to the zero phase, marking the interface between biogenic limestone and igneous rock. H2 is calibrated at the zero crossing of the seismic wavelet, delineating the boundary between high- and medium-amplitude strata. H3 represents the interface between the carbonate platform and the bioclastic shoal, marking the boundary of the carbonates cycle. B2 signifies the interface

between limestone and igneous rock, representing the top of the volcanic edifice. H4 marks the base of the volcanic edifice, which also represents the initiation of the complex buildup. B3 is the interface between calcareous sandstone and sandstone, while H5 corresponds to the boundary between sandstone and igneous rock. The seismic interpretation was calibrated using Well A, where synthetic traces closely matched the characteristics of the PSTM seismic profile, ensuring a reliable calibration with a reasonable time-depth relationship.

4.3 Seismic units

The depositional architecture of the Baiyun Sag central complex buildup is highly heterogeneous due to the multi-period volcanic activity that occurred during the development of the carbonate platform. To define the seismic unit framework of this buildup, this study utilized secondary three-dimensional PSDM data covering approximately 300 km². Based on well-to-seismic calibration, the seismic units of the complex buildup exhibit a three-segment reflection pattern (Figure 6A). Unit 3 displays weak amplitude and overall poor continuity seismic reflection pattern. Unit 2 presents medium amplitude and poor continuity, with a set of medium-strong trough and strong amplitude reflectors developed at the top. Unit 1 is characterized by strong amplitude and relatively high continuity. Carbonates are symmetrically developed around the platform, showing a lateral accretion pattern.

The central part of the platform features a flat-topped morphology in the seismic profile b-b' (Figure 6A), while the

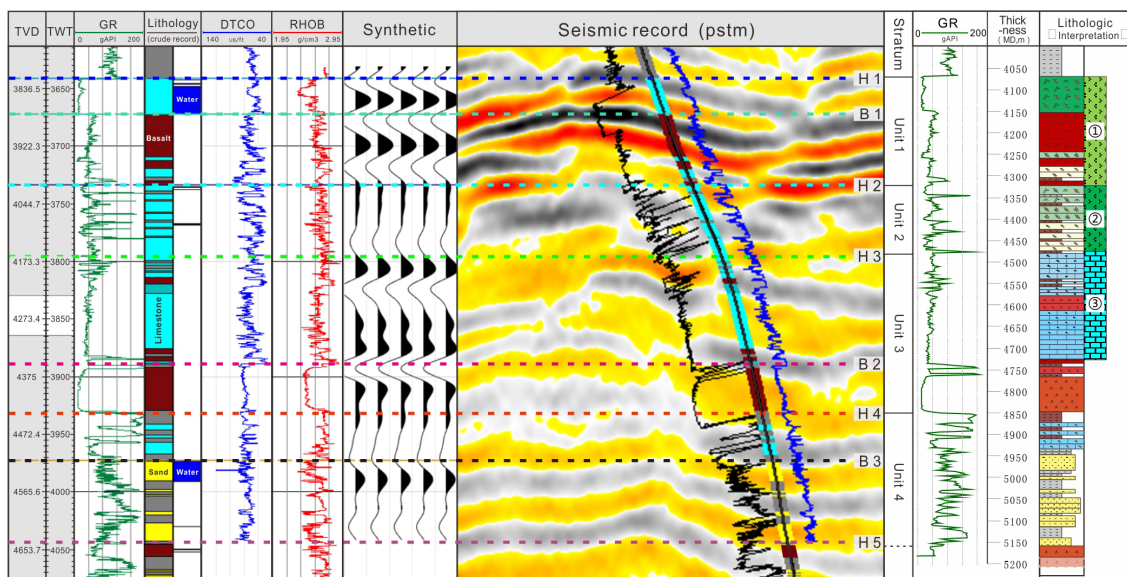


FIGURE 5

Well-to-Seismic Calibration: Five key horizons (H1-H5) and three lithological boundaries (B1-B3) were identified during the calibration. Four stratum units were identified and named Zhujiang units 1-4. From bottom to top, Unit 4 predominantly consists of calcareous and tuffaceous sandstones, showing a disordered GR curve; Unit 3 is composed of both igneous rocks and carbonates, with low GR values for both lithologies, and the corresponding GR curves exhibit a box-like shape; Unit 2 is characterized by bioclastic limestone interbedded with thin layers of claystone, displaying a series of single-peak shapes on the GR curve with high values; Unit 1 features alternating layers of igneous rocks and carbonates. The igneous rocks show a jagged profile with low GR values, while the carbonates present a box-like shape with the lowest GR values.

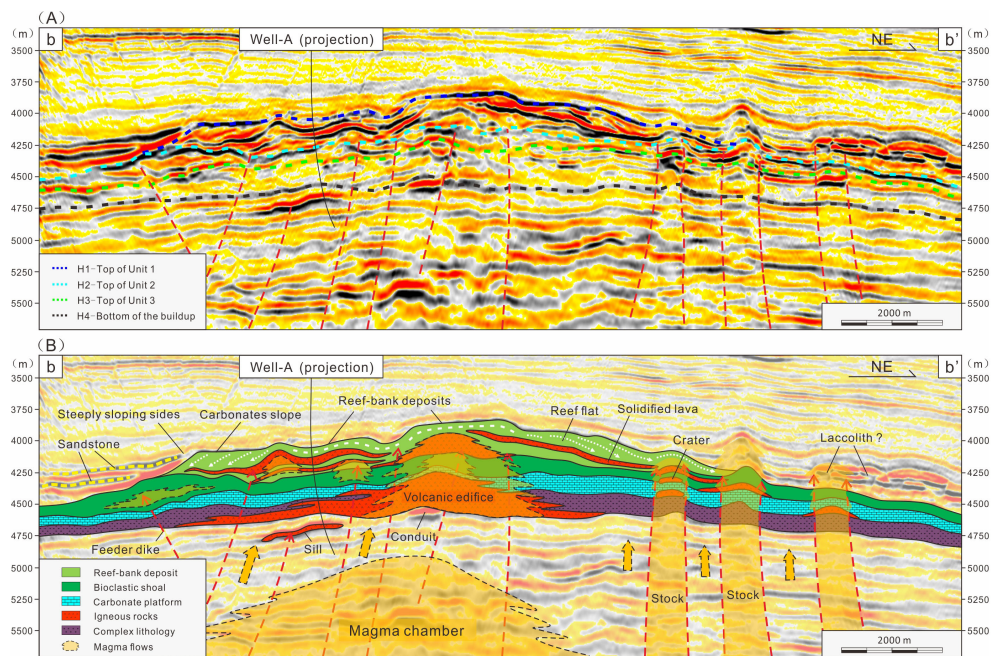


FIGURE 6

Interpretation of Seismic Profile b-b': (A) shows the original seismic section, and (B) shows the corresponding lithological interpretation. The calibration results indicate that the seismic reflection structure of the complex buildup exhibits a distinct three-segment pattern, characterized by "strong-moderate-weak" amplitude variations. Unit 3 shows weak amplitude and poor continuity in its seismic reflections. Unit 2 displays medium amplitude and weak continuity, with a set of relatively continuous trough reflections at the top. Unit 1 is characterized by strong amplitude reflections, with a relatively steep slope observed along the southwestern edge of the platform. Laterally, sheet-like sandstone deposits are observed around the buildup.

flanks exhibit a lateral accretion pattern on both sides of the paleo-high, characteristics of a carbonate platform (Pomar et al., 2012). The southwestern margin of the platform displays a relatively steep slope, interpreted as a carbonate slope. Drilling results from the periphery indicate the development of sheet-like sand bodies around the buildup, as shown by the yellow dotted line on the southwestern side of the seismic profile in Figure 6B. Additionally, late-stage intrusive rocks on the northeastern side of the platform have pierced the buildup, altering the morphological configuration of the overlying strata.

In the seismic profile c-c' shown in Figure 7A, a chaotic, dome-shaped seismic facies at the base of the buildup is interpreted as the magma chamber sourced from the deep mantle. This magma chamber serves as the material source for igneous rock activity above the buildup, with the magma being transported through volcanic conduits (Figure 7B). Lithological analysis from Well A indicates that a volcanic edifice developed in the lower part of Unit 3, creating a local paleogeographic high. Above this, the upper part of Unit 3 consists of thick limestone, characteristic of a carbonate platform. In Unit 2, bioclastic shoal deposits are found at the crests of the platform, while the lower part of the platform exhibits a gradual transition from biogenetic limestone to micrite limestone. During the deposition of reef-bank sediments in Unit 1, significant fault development occurred, which facilitated the transport of magma into the shallow (Magee et al., 2013). Magma from fissure eruptions formed isolated, sheet-like bodies that became intercalated with the biogenetic limestone. Unit 1 displays varying degrees of slope around

the platform, interpreted as the carbonate platform margin. A large set of weak to absent reflections above the buildup suggests the deposition of mudstone in a semi-bathyal environment.

In the seismic profile d-d' shown in Figure 8A, the entire buildup exhibits a hypotenuse-triangle shape, with stratigraphic units displaying well-defined layering. The southeast side of the buildup features a steeper slope, while the northwest side presents a gentler slope. The main volcanic vent (Figure 8B) is situated in the central diapir zone of the Baiyun Sag, which is characterized by dense faulting that has penetrated the complex on the southeast side of the profile. The projection of Well A in Unit 1 is located in the middle-high geomorphic region of the buildup. It is observed that sheet-like magma has overflowed from the central diapir zone. Overlying these solidified magma units, a set of biogenic limestones has developed. In the context of continuous marine transgression, it can be reasonably inferred that the biogenic limestone migrated upwards, eventually covering the entire platform's high points. The seismic fuzzy zone, characterized by a series of fault-related microcracks, suggests ongoing volcanic conduit activity in the later stages. This activity facilitated the transport of hydrothermal fluids and gases into the shallow strata.

4.4 Seismic facies

Carbonate and igneous buildups share similar seismic characteristics, making their differentiation a persistent challenge.

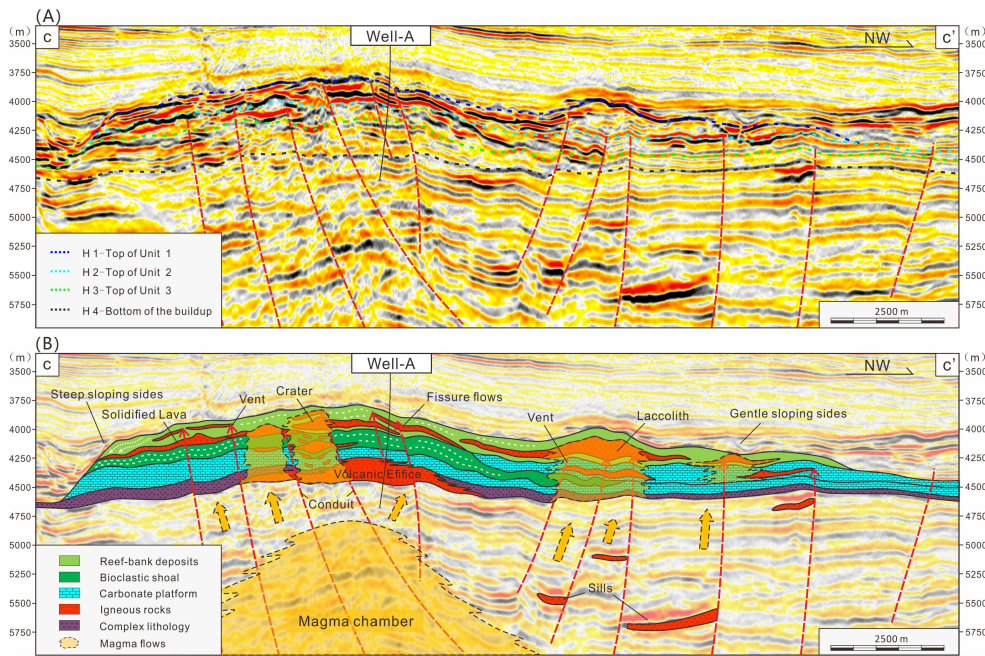


FIGURE 7

Interpretation of seismic profiles c-c'. (A) shows the original seismic section, and (B) shows the corresponding lithological interpretation. The complex buildup is primarily divided into three units. In the lower part of Unit 3, the igneous edifice is located at the center, while the purple strata represent a complex lithology of tuffaceous sandstone formed during the same period. In the upper part of Unit 3, carbonates developed in relatively deeper water conditions. In Unit 2, bioclastic shoals are present at the crest of the buildup, while limestone is distributed in the lower part. The biogenic limestone in Unit 1 is depicted in light green. Faults serve as vents for the intrusion and eruption of igneous rocks into the shallow strata, with sheet-like igneous sills observable in the deep areas surrounding the faults.

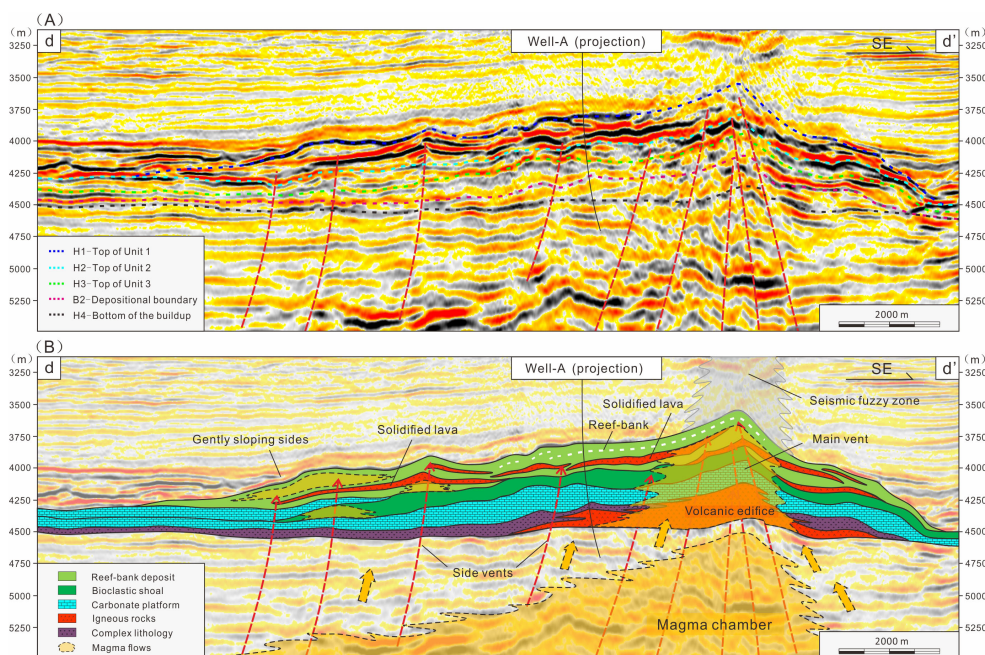


FIGURE 8

Interpretation of seismic profiles d-d'. (A) shows the original seismic section, and (B) shows the corresponding lithological interpretation. On the right side of the drilling well, the central dispair zone is influenced by shallow gas, resulting in relatively poor seismic imaging. The buildup shows a gentler slope on the northwest side (d) and a steeper slope on the southeast side (d'). The projection point of Well A is located in the middle-high geomorphic region of the platform. The seismic events intersecting Well A exhibit strong continuity and extend into the seismic fuzzy zone with reduced clarity.

This study leverages comprehensive lithological data and well-seismic calibration to provide valuable insights into distinguishing carbonates from igneous rocks based on seismic facies. Eight types of seismic facies (SF) are identified and classified according to reflection properties such as amplitude, continuity, internal configuration, and external geometry (Table 2). SF1 to SF4 correspond to igneous-related facies, which include volcanic edifices, solidified lava, volcanic conduits, and intrusive stocks. In contrast, SF5 to SF8 represent carbonate-related facies, such as reef-bank systems, reef-flat deposits, carbonate slopes, and carbonate platforms. Igneous seismic facies display greater vertical variability (Planke et al., 2005), reflecting the influence of magma supply from deeper sources. In comparison, carbonate seismic facies are characterized by more horizontal accumulation and migration, driven primarily by fluctuations in relative sea level.

The volcanic edifice exhibits a convex geometry in seismic profiles (SF1 in Table 2). The crater at the top forms a circular seismic feature, with the main vent characterized by strong amplitude reflections at the center. The flanks display medium to weak amplitude reflections with subparallel structures, typically composed of lava or pyroclastic materials.

The solidified lava is characterized by isolated, elongated sheet-like geometries (SF2 in Table 2), typically extending 1-2 km. Lava units display high amplitude and continuous reflections (Hansen and Cartwright, 2006). SF2 is interpreted as lava flow units interbedded with biogenetic limestone. The development of overflow magma is closely related to fault activity, which provides pathways for magma transport from the deep magma chamber.

The volcanic conduit has a cylindrical external shape, with internal seismic facies exhibiting low amplitude, discontinuous, and chaotic reflections (SF3 in Table 2). The largest volcanic conduit is located in the southwestern part of the buildup and serves as the primary source of the volcanic edifice. This conduit is characterized by dense faults and microcracks, which act as the main pathways for magma transport from deep to shallow areas.

The intrusive stock is associated with low amplitude, semi-continuous, and chaotic reflections (SF4 in Table 2). These stocks typically show weak amplitude and chaotic reflections due to poor stratification. Localized stocks have penetrated the buildup, significantly altering the morphology of the overlying strata. These intrusions are often associated with faults (Hansen and Cartwright, 2006), linking to deeper strata, where sills develop along the fault zones.

The reef-bank deposits exhibit a typical mound-like geometry (SF5 in Table 2), with greater thickness at the center and tapering towards the sides, indicating sedimentation from reef-bank deposits. Internally, SF5 is characterized by low amplitude, semi-continuous, and partly discontinuous reflections. Thin samples from Well A confirm the presence of biogenetic limestone associated with reef-bank deposits, with coral fragments observed in the drill cuttings.

The reef-flat clinoform has a wedge-shaped geometry with lateral accretion patterns (SF6 in Table 2). These are characterized by high amplitude, moderately to highly continuous reflections, interpreted as reef-flat deposits. SF6 and SF7 developed

symmetrically on the high landform, with SF6 exhibiting a relatively gentle slope.

The carbonate slope exhibits a typical platform margin geometry, with laterally aggradational reflection configurations (SF7 in Table 2). It is characterized by high amplitude and continuous reflections, resembling distally steepened ramps (Pomar et al., 2012). The profile of SF7 presents a relatively steep slope at the carbonate platform edge.

The carbonate platform shows parallel to subparallel seismic reflections, with low amplitude and semi-continuous characteristics (SF8 in Table 2). The seismic reflection patterns of the carbonate platform align with low-angle homoclinal ramp types (Pomar et al., 2012). Drill cuttings from Well A indicate that the carbonate platform is partly composed of mixed sediments, primarily tuffaceous limestone and micrite limestone.

5 Discussion

5.1 Evolution of the complex buildup

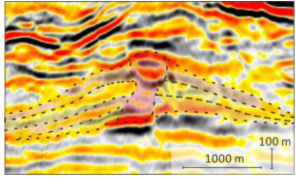
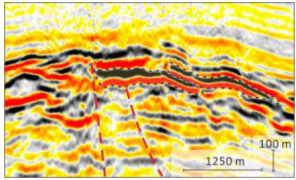
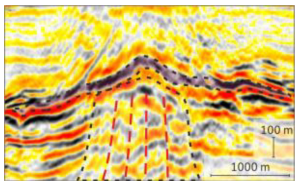
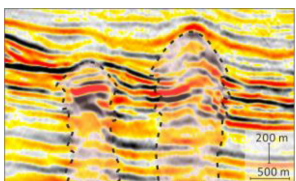
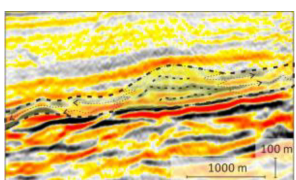
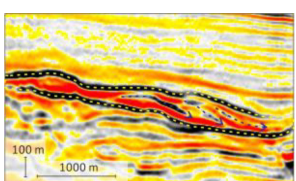
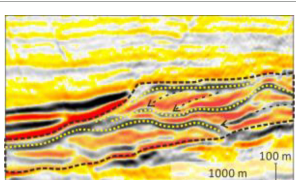
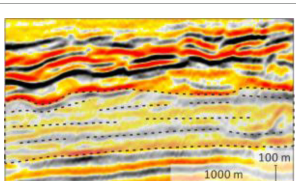
The Pearl River Mouth Basin is a large detachment basin, with the Baiyun Sag situated in the necking zone of crustal thinning (Ren et al., 2015; Pang et al., 2018). During the Oligocene to Miocene periods, significant igneous activity occurred in the region (Yan et al., 2006). The formation of the central diapir in the Baiyun Sag is linked to the intrusion of magma from the deep mantle into shallower strata, altering the regional topography and creating a gently domed surface morphology (Montanari et al., 2017). Volcanic eruptions initiated the formation of igneous edifices, marking the beginning of the buildup's development.

The formation of the complex buildup can be divided into three primary stages: (I) Volcanic eruptions and carbonates development, (II) overflowing magma and reef shoal deposits, and (III) reef-bank deposition accompanied by igneous intrusion. These stages can further be broken down into six key periods: (a) volcanic mound formation; (b) carbonate platform development; (c) intermittent volcanic eruptions; (d) wave-dominated bioclastic shoal; (e) shallow igneous intrusions; (f) reef-bank development. Ultimately, as relative sea levels rose, platform development ceased, and the buildup was subsequently covered by thick hemipelagic sediments.

5.1.1 Volcanic eruptions and carbonates development

The first period is marked by volcanic eruptions (Figure 9A), which occurred underwater, leading to the accumulation of pyroclastic deposits near the crater. These deposits formed a volcanic mound, with alternating layers of lava and ash on the mound's flanks. Surrounding sediments consisted of a mix of tuffaceous and calcareous sandstones. The eruption created a local paleogeographic high, and lava overflow, along with shallow igneous intrusions, developed at the top of the buildup, providing a solid substrate conducive to carbonate growth. In the second stage, the carbonate platform began to develop (Figure 9B). This process is similar to the formation of carbonate platforms in the

TABLE 2 Seismic facies with associated features identified from the complex buildup.

Seismic facies	Example	Internal reflection pattern	Configuration and geometry	Lithofacies Interpretation
SF1		Medium to high amplitude, semi-continuous reflection	Mounded, Slight concave flank	Eruptive rock/ Volcanic edifice
SF2		High amplitude, continuous reflection	Isolated-sheeted	Effusive rock/ Solidified lava
SF3		Low amplitude, discontinuous, chaotic reflection	Columnar	Volcanic rock/ Conduit
SF4		Low amplitude, semi-continuous to partly discontinuous, chaotic reflection	Columnar Change the overlying stratum morphology	Intrusive rock/ Stock
SF5		Low amplitude, semi-continuous to partly discontinuous reflection	Mounded	Biogenetic limestone/ Reef-bank deposits
SF6		High amplitude, continuous to semi-continuous reflection	Wedge, slight convex-up, progradation	Biogenetic limestone/ Reef-flat cliniform
SF7		High amplitude, continuous to semi-continuous reflection	Steep slope, progradation	Limestone/ Carbonate slope
SF8		Low amplitude, semi-continuous to partly discontinuous, sub-parallel reflection	Sheeted, Parallel styles	Limestone/ Carbonate platform

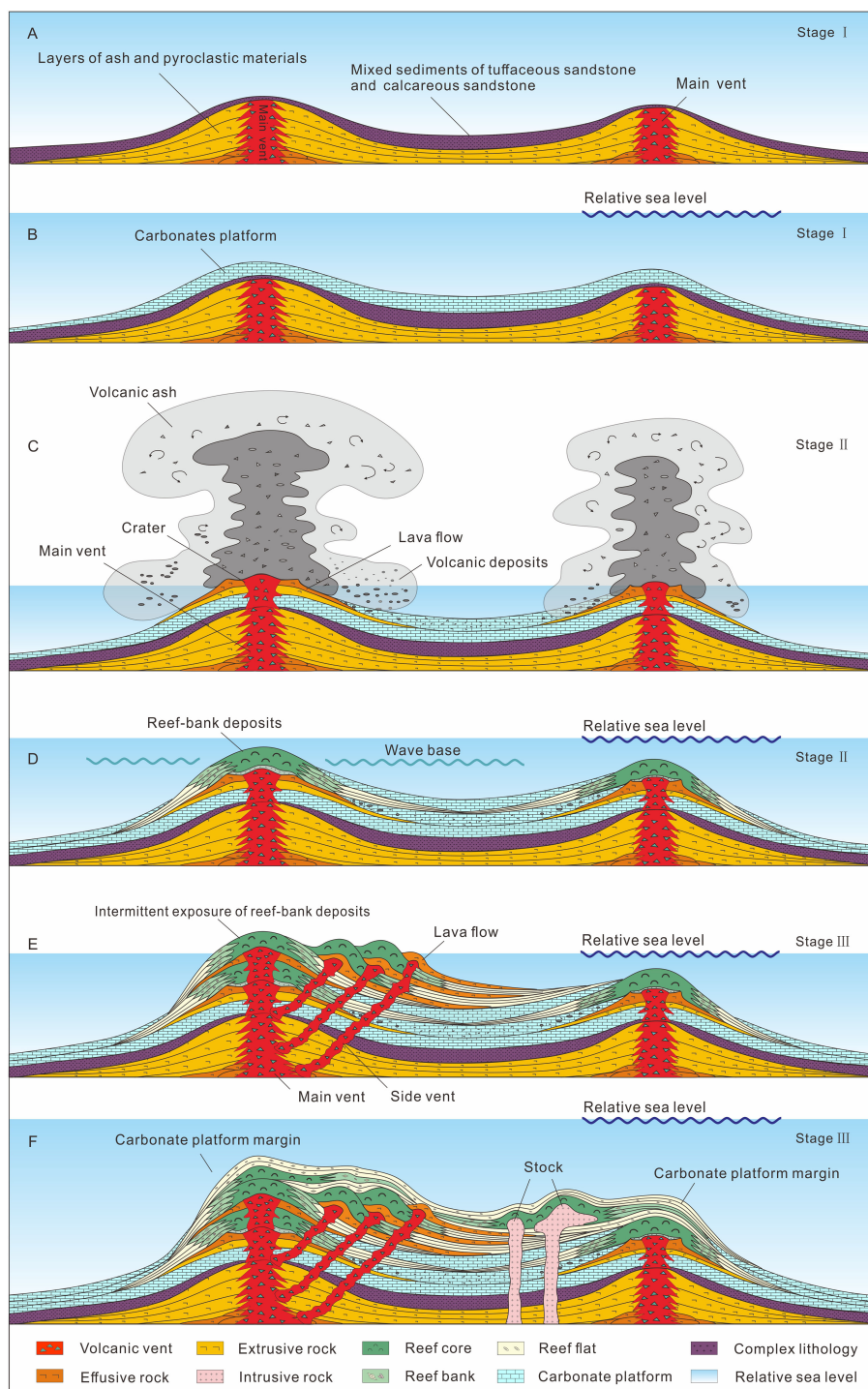


FIGURE 9

The evolutionary model diagram of the complex buildup illustrates the platform's evolution through six distinct periods. (A) Volcanic mound formation: This stage is characterized by underwater explosive eruptions, leading to the formation of the volcanic mound.; (B) The volcanic mound provided a paleogeographic high, facilitating the development of carbonates in a shallow marine environment; (C) Intermittent volcanic eruptions stage. Continuous volcanic activity during this stage led to the formation of sheet-like lava during the overflow phase, with large amounts of tuff mixed into the limestone; (D) Wave-dominated bioclastic shoal. Reef flat facies sediments developed, with the limestone containing abundant biological debris, indicating a shallow water environment on the platform; (E) Shallow igneous intrusion. Fissure vents formed multiple layers of overflow-facies lava sheets on the platform; (F) Development of reef-bank. As relative sea level rises, the reef bank system migrates to the paleo-high position and the platform development ceased. Late-stage intrusive rock development occurred during this phase.

South China Sea, both evolving in volcanic settings (Wu et al., 2021; Liu et al., 2022; Zhang et al., 2024). During this period, thick layers of micrite limestone with low biological content accumulated on the platform. The higher portions of the buildup were no longer influenced by clastic sandstone, providing favorable conditions for carbonate. By the end of this stage, tuffaceous particles began appearing in the limestone, signaling continued volcanic activity in the region.

5.1.2 Overflowing magma and reef shoal deposits

During the third period, both igneous rocks and carbonates developed on the platform (Figure 9C). In the early phase, volcanic activity was intense, leading to overflow magma formation around the crater. Away from the volcanic influence, extensive carbonate strata interspersed with tuffaceous layers were deposited. In the later phase, bioclastic micrite limestone, formed in the central part of the platform, reflecting a restricted environment with weak hydrodynamic conditions. Small reefs began to form along the platform edge. As igneous activity waned and relative sea levels rose, the platform transitioned to a carbonate-dominated stage. The fourth period occurred in a shallow-water environment with strong hydrodynamic conditions (Figure 9D). Bioclastic limestone was deposited, with thin layers of claystone and mudstone interspersed. The limestone had relatively low cement content, and the extensive fragmentation of foraminifera, red algae, and mollusk indicated significant wave action. The carbonate strata developed in this shallow environment were vulnerable to exposure and dissolution during sea-level fluctuations. Notably, during this period, igneous activity on the platform diminished, and the lithology was primarily limestone and claystone, leading to weak seismic reflection amplitudes.

5.1.3 Reef-bank deposition accompanied by igneous intrusion

The fifth period saw the platform evolve into an isolated carbonate platform, conducive to the formation of reefal limestone (Figure 9E). These shallow-water, tropical carbonate platforms were dominated by corals, benthic foraminifera, algae, and mollusks (Jorry et al., 2016; Prat et al., 2016). The biogenetic limestone in this phase had a high cement content. Simultaneously, shallow igneous intrusions occurred through secondary vents, while effusive lava flowed through fissures. Faults became the main pathways for shallow magma intrusion, resulting in numerous side vents within the buildup. Lava flows spread across the surface, solidifying into hardground surfaces, and providing stable substrates for reef development.

The sixth period marked the demise of the carbonate platform (Figure 9F). As relative sea levels rose, the reef-bank system gradually migrated towards the higher regions of the buildup, reducing the size of the carbonate platform. A relatively thin sequence of dense limestone developed at the platform's top (Henglai et al., 2024). As the buildup subsided into deeper waters, platform development ceased, and the area was covered by semi-pelagic mudstone. Sand bodies associated with contour currents were observed around the buildup. As the buildup sank

further into the deep sea, it became increasingly covered during or after this period, significantly altering the morphology of the overlying strata.

5.2 Discriminating volcanic rocks from carbonates

From a geological time scale, the development of carbonate platforms is gradual, whereas igneous activity is more instantaneous (Tang et al., 2015). Surface volcanic rock and underground intrusive bodies are interconnected (Burchardt, 2018), suggesting that identifying volcanic rocks requires examining the volcanic and igneous plumbing system. These structures often include magma vents that link deep magma chambers (typical of Figure 6B, 7B), with eruptions at the surface or intrusions into shallow strata. Identifying volcanic vents and fault systems helps to map the distribution of igneous rocks within complex buildups.

In the study area, volcanic mounds show various seismic facies, such as volcanic vents, tuff cones, and forest units, with pyroclastic deposits, mound-top shoals, and basinal hemipelagics typically found near the volcanic edifice (Ma et al., 2018a). These characteristics are critical for identifying igneous facies in this study. Seismic facies associated with igneous rocks (SF1 - SF4), reflect their connection to volcanic conduits or fault systems, demonstrating a strong vertical communication with deep magma chambers.

In contrast, carbonate platforms are primarily influenced by tectonic activity and eustatic sea-level fluctuations, typically exhibiting subparallel sequence units (Fournier et al., 2005; Wu et al., 2014; Shahzad et al., 2018; Henglai et al., 2024). Seismic facies of carbonate platforms display a variety of geomorphic features, such as low-angle homo-clinal morphologies, distal steepening slopes, flat-topped platforms, and reef-edge shelves (Bosence, 2005). These features correspond to carbonate-related seismic facies SF5–SF8. Furthermore, the top of carbonate platforms often display a sub-flat or flat-topped morphology, with aggradation along the platform flanks and backstepping along the margins (Liu et al., 2023). These distinctive characteristics are clearly illustrated in Figure 6, providing a valuable guide for identifying carbonate formations.

5.3 Implications for oil and gas exploration

Igneous rocks as seen in samples from Well A, lack pore structures and do not exhibit the typical characteristics of oil and gas reservoirs within complex buildups (Table 1). The igneous rocks in shallow intrusive or effusive facies are dense and have negligible porosity (Figures 4B, D–F). While the eruptive rocks may contain original pores, these pores are fully cemented by Fe-dolomite (Figures 4A, C, I). Though igneous rocks themselves cannot serve as reservoirs, magma supply systems may function as pathways for oil and gas migration (Svensen et al., 2004). Additionally, volcanic conduit, characterized by dense fractures and ongoing activity over

multiple geological periods, could potentially act as oil and gas reservoirs. However, the reservoir properties of volcanic conduits have not been confirmed by Well A, leaving uncertainty about their porosity and permeability conditions.

Carbonate lithofacies exhibit considerable variabilities in porosity and permeability (Li et al., 2018). Understanding the relationship between depositional architectures and lithofacies heterogeneities on carbonate platforms enhances the interpretation of paleoenvironmental evolution and aids in predicting reservoir properties (Leonide et al., 2012; Chen et al., 2018, 2024). Carbonate successions exhibit distinct depositional profiles and facies-belt distributions, which can be effectively predicted using comparative sedimentology and seismic facies analysis (Pomar and Kendall, 2008). Coral framestone generally demonstrates the highest reservoir quality, followed by bioclastic packstone/wackestone, while micrite limestone and interbedded shale-limestone have poor reservoir quality (Makhankova et al., 2020; Henglai et al., 2024). This pattern is consistent with the rock samples from Well A, where Unit 1 shows reservoir properties compared to Unit 2, which in turn is better than Unit 3.

6 Conclusion

1. The complex buildup in the Baiyun Sag comprises both igneous rocks and carbonates. Its evolution can be divided into three main stages: a) volcanic eruptions and carbonates development; b) overflowing magma and reef shoal deposits, and c) reef-bank deposition accompanied by igneous intrusion. This evolutionary process reflects the transition of carbonate platforms from deep-water to shallow-water environments, alongside the progression of igneous activity from extrusive to intrusive facies.

2. Seismic facies associated with igneous rocks can be categorized into eruptive, effusive, and intrusive facies. Eruptive and intrusive facies are characterized by low-amplitude, discontinuous, and chaotic reflections, while effusive facies are distinguished by high-amplitude, continuous reflections. Seismic facies of reefal carbonates typically exhibit high-amplitude, continuous reflections at the outer contours, with weak reflection and low continuity in the interior, while carbonate platforms feature as low-amplitude and low continuity.

3. To identify complex buildups, igneous rocks can be distinguished by fault and volcanic conduits, whereas carbonates display more pronounced stratification away from igneous activity. Carbonates typically present a symmetrical structure on both sides of the highland, with gentle slopes in the reef flat cliniform and steeper slopes along the platform margin. In contrast, volcanic mounds exhibit concave, gentle slopes.

4. Volcanic activity influences landform development, creating paleogeographic highs that provide favorable conditions for carbonate growth. As relative sea levels rise, reef-bank systems progressively migrate toward these elevated areas of the platform. Frequent fluctuations in relative sea level make the biogenic limestone in these paleogeographic highs susceptible to

weathering and dissolution, processes that contribute to the formation of effective oil and gas reservoirs.

Data availability statement

The datasets presented in this article are not readily available because the data utilized in this study were provided by the Shenzhen Branch of China National Offshore Oil Corporation Ltd under confidential status. Requests to access the datasets should be directed to polaristar@foxmail.com.

Author contributions

BC: Conceptualization, Data curation, Investigation, Writing – original draft, Writing – review & editing. LX: Investigation, Supervision, Writing – original draft. BL: Investigation, Writing – review & editing. LZ: Investigation, Supervision, Writing – review & editing. DX: Investigation, Writing – review & editing. YG: Investigation, Writing – original draft, Writing – review & editing. FW: Investigation, Writing – original draft. XY: Investigation, Writing – original draft. YLZ: Investigation, Writing – review & editing. YM: Investigation, Writing – review & editing. YMZ: Investigation, Writing – review & editing.

Funding

The author(s) declare that no financial support was received for the research, authorship, and/or publication of this article.

Acknowledgments

We are grateful to Shenzhen Branch of China National Offshore Oil Corporation Ltd for the permission to release the data used in this work.

Conflict of interest

Authors BC, LX, BL, LZ, DX, XY, YMZ, YM, and YLZ were employed by Shenzhen Branch of China National Offshore Oil Corporation Ltd.

The remaining authors declare that the research was conducted in the absence of any commercial or financial relationships that could be construed as a potential conflict of interest.

Generative AI statement

The author(s) declare that no Generative AI was used in the creation of this manuscript.

Publisher's note

All claims expressed in this article are solely those of the authors and do not necessarily represent those of their affiliated

organizations, or those of the publisher, the editors and the reviewers. Any product that may be evaluated in this article, or claim that may be made by its manufacturer, is not guaranteed or endorsed by the publisher.

References

- Atasoy, S. G., Altiner, D., and Okay, A. I. (2018). Reconstruction of a Late Jurassic–Early Cretaceous carbonate platform margin with composite biostratigraphy and microfacies analysis (western Sakarya Zone, Turkey): Paleogeographic and tectonic implications. *Cretac. Res.* 92, 66–93. doi: 10.1016/j.cretres.2018.07.009
- Bachtel, S. L., Posamentier, H. W., and Gerber, T. P. (2010). “Seismic Geomorphology and Stratigraphic Evolution of a Tertiary-Aged Isolated Carbonate Platform System, Browse Basin, North West Shelf of Australia—Part II,” in *Seismic Imaging of Depositional and Geomorphic Systems*. Eds. L. J. Wood, T. T. Simo and N. C. Rosen (Houston, Texas, USA: SEPM Society for Sedimentary Geology), 0. doi: 10.5724/gcs.10.30.0115
- Betzler, C., Fürstenau, J., Lüdmann, T., Hübscher, C., Lindhorst, S., Paul, A., et al. (2013). Sea-level and ocean-current control on carbonate-platform growth, Maldives, Indian Ocean. *Basin Res.* 25, 172–196. doi: 10.1111/j.1365-2117.2012.00554.x
- Bosence, D. (2005). A genetic classification of carbonate platforms based on their basinal and tectonic settings in the Cenozoic. *Sedimentary Geol.* 175, 49–72. doi: 10.1016/j.sedgeo.2004.12.030
- Burchardt, S. (2018). Introduction to volcanic and igneous plumbing systems—Developing a discipline and common concepts[M]/Volcanic and igneous plumbing systems. *Elsevier* 2018, 1–12. doi: 10.1016/B978-0-12-809749-6.00001-7
- Burgess, P. M., Winefield, P., Minzoni, M., and Elders, C. (2013). Methods for identification of isolated carbonate buildups from seismic reflection data. *AAPG Bull.* 97, 1071–1098. doi: 10.1306/12051212011
- Chen, B., Wu, F., Xie, X., Gao, Y., and Wang, X. (2024). Sequence stratigraphic analysis of the late Permian Changhsingian platform marginal reef, Western Hubei, South China. *Front. Mar. Sci.* 11. doi: 10.3389/fmars.2024.1470867
- Chen, B., Xie, X., Al-Aasm, I. S., Wu, F., and Zhou, M. (2018). Depositional architecture and facies of a complete reef complex succession: a case study of the Permian Jianbianba Reefs, Western Hubei, South China. *Minerals* 8, 533. doi: 10.3390/min8110533
- Chiarella, D., and Longhitano, S. G. (2012). Distinguishing depositional environments in shallowwater mixed bio-siliciclastic deposits on the base of the degree of heterolithic segregation (Gelasian, southern Italy). *J. Sediment. Res.* 82, 969–990. doi: 10.2110/jsr.2012.78
- Coletti, G., Basso, D., Betzler, C., Robertson, A. H. F., Bosio, G., El Kateb, A., et al. (2019). Environmental evolution and geological significance of the Miocene carbonates of the Eratosthenes Seamount (ODP Leg 160). *Palaeogeogr. Palaeoclimatol. Palaeoecol.* 530, 217–235. doi: 10.1016/j.palaeo.2019.05.009
- Counts, J. W., Jorry, S. J., Leroux, E., Miramontes, E., and Jouet, G. (2018). Sedimentation adjacent to atolls and volcano-cored carbonate platforms in the Mozambique Channel (SW Indian Ocean). *Mar. Geol.* 404, 41–59. doi: 10.1016/j.margeo.2018.07.003
- Courgeon, S., Jorry, S. J., Camoin, G. F., BouDagher-Fadel, M. K., Jouet, G., Révillon, S., et al. (2016). Growth and demise of Cenozoic isolated carbonate platforms: New insights from the Mozambique Channel seamounts (SW Indian Ocean). *Mar. Geol.* 380, 90–105. doi: 10.1016/j.margeo.2016.07.006
- Courgeon, S., Jorry, S. J., Jouet, G., Camoin, G., BouDagher-Fadel, M. K., Bachèlery, P., et al. (2017). Impact of tectonic and volcanism on the Neogene evolution of isolated carbonate platforms (SW Indian Ocean). *Sedimentary Geol.* 355, 114–131. doi: 10.1016/j.sedgeo.2017.04.008
- Deng, P., Mei, L., Liu, J., Zheng, J., Liu, M., Cheng, Z., et al. (2019). Episodic normal faulting and magmatism during the syn-spreading stage of the Baiyun sag in Pearl River Mouth Basin: response to the multi-phase seafloor spreading of the South China Sea. *Mar. Geophysical Res.* 40, 33–50. doi: 10.1007/s11001-018-9352-9
- Dimou, V.-G., Koukousioura, O., Less, G., Triantaphyllou, M. V., Dimiza, M. D., Strydes, G., et al. (2024). Microfacies and species richness analysis of upper Bartonian and Priabonian carbonate shelf deposits from the Thrace Basin (Tethyan Ocean, Greece): Paleoenvironmental evolution and species-richness hotspot revealed. *Mar. Pet. Geol.* 170, 107126. doi: 10.1016/j.marpetgeo.2024.107126
- Dunham, R. J. (1962). “Classification of Carbonate Rocks According to Depositional Textures,” in *AAPG Memoir*, vol. 1, 108–121.
- Feng, Z., and Zheng, W. (1982). Tectonic evolution of Zhujiangkou (Pearl River Mouth) Basin and origin of South China Sea. *Acta Geol. Sin.* 56, 212–222.
- Fournier, F., Borgomano, J., and Montaggioni, L. F. (2005). Development patterns and controlling factors of Tertiary carbonate buildups: Insights from high-resolution 3D seismic and well data in the Malampaya gas field (Offshore Palawan, Philippines). *Sedimentary Geol.* 175, 189–215. doi: 10.1016/j.sedgeo.2005.01.009
- Greenlee, S. M., and Lehmann, P. J. (1993). “Stratigraphic framework of productive carbonate buildups,” in *Carbonate Seq. Stratigr. Recent Dev. Appl.*, 43–62.
- Hansen, D. M., and Cartwright, J. (2006). The three-dimensional geometry and growth of forced folds above saucer-shaped igneous sills. *J. Struct. Geol.* 28, 1520–1535. doi: 10.1016/j.jsg.2006.04.004
- Henglai, P., Fongngern, R., and Saller, A. (2024). The growth and demise of a Middle Miocene carbonate platform in Central Luconia, offshore Malaysia. *Mar. Petroleum Geol.* 163, 106763. doi: 10.1016/j.marpetgeo.2024.106763
- Insalaco, E. (1998). The descriptive nomenclature and classification of growth fabrics in fossil scleractinian reefs. *Sedimentary Geol.* 118, 159–186. doi: 10.1016/S0037-0738(98)00011-6
- Isern, A. R., Anselmetti, F. S., and Blum, P. (2004). “A Neogene Carbonate Platform, Slope, and Shelf Edifice Shaped by Sea Level and Ocean Currents, Marion Plateau (Northeast Australia),” in *Seismic Imaging of Carbonate Reservoirs and Systems*. Eds. G. P. Eberli, J. L. Masafferro and J. F. “Rick” Sarg (Tulsa, OK, USA: American Association of Petroleum Geologists), 0. doi: 10.1306/M81928
- Jorry, S. J., Camoin, G. F., Jouet, G., Roy, P. L., Vella, C., Courgeon, S., et al. (2016). Modern sediments and Pleistocene reefs from isolated carbonate platforms (Iles Eparses, SW Indian Ocean): a preliminary study. *Acta oecologica* 72, 129–143. doi: 10.1016/j.actao.2015.10.014
- Klován, J. E., and Embry, A. F. III (1972). Absolute water depth limits of Late Devonian paleoecological zones. *Geol. Rundsch.* 61, 672–686. doi: 10.1007/BF01896340
- Leonide, P., Borgomano, J., Masse, J. P., and Doublet, S. (2012). Relation between stratigraphic architecture and multi-scale heterogeneities in carbonate platforms: The Barremian–lower Aptian of the Monts de Vaucluse, SE France. *Sedimentary Geol.* 265, 87–109. doi: 10.1016/j.sedgeo.2012.03.019
- Li, C., Li, J., Ding, W., Franke, D., Yao, Y., Shi, H., et al. (2015). Seismic stratigraphy of the central South China Sea basin and implications for neotectonics. *J. Geophysical Res.: Solid Earth* 120, 1377–1399. doi: 10.1002/2014JB011686
- Li, R., Qiao, P., Cui, Y., Zhang, D., Liu, X., Shao, L., et al. (2018). Composition and diagenesis of Pleistocene aeolianites at Shidao, Xisha Islands: Implications for palaeoceanography and palaeoclimate during the last glacial period. *Palaeogeogr. Palaeoclimatol. Palaeoecol.* 490, 604–616. doi: 10.1016/j.palaeo.2017.11.049
- Liu, J., Cao, L., Xu, W., Li, G., Xiang, S., Luo, Y., et al. (2022). Formation and development of coral reefs in the South China Sea. *Palaeogeogr. Palaeoclimatol. Palaeoecol.* 594, 110957. doi: 10.1016/j.palaeo.2022.110957
- Liu, G., Wu, S., Gao, J., Zhang, H., Han, X., Qin, Y., et al. (2023). Seismic architecture of yongle isolated carbonate platform in xisha archipelago, south China Sea. *Front. Earth Sci.* 11. doi: 10.3389/feart.2023.1100675
- Luo, K., Su, M., Liu, S., Shi, J., Wang, C., Chen, H., et al. (2023). Sea-level, climate, and oceanographic controls on recent deepwater hyperpycnites: A case example from the shenhu slope (northern South China Sea). *Quat. Sci. Rev.* 311, 108148. doi: 10.1016/j.quascirev.2023.108148
- Ma, B., Wu, S., Betzler, C., Qin, Z., Mi, L., Gao, W., et al. (2018a). Geometry, internal architecture, and evolution of buried volcanic mounds in the northern South China Sea. *Mar. Pet. Geol.* 97, 540–555. doi: 10.1016/j.marpetgeo.2018.07.029
- Ma, B., Wu, S., Mi, L., Lüdmann, T., Gao, J., and Gao, W. (2018b). Mixed carbonate-siliciclastic deposits in a channel complex in the northern South China sea. *J. Earth Sci.* 29, 707–720. doi: 10.1007/s12583-018-0830-4
- Ma, B., Wu, S., Sun, Q., Mi, L., Wang, Z., and Tian, J. (2015). The late Cenozoic deep-water channel system in the Baiyun Sag, Pearl River Mouth Basin: Development and tectonic effects. *South China Sea Deep* 122, 226–239. doi: 10.1016/j.ds2.2015.06.015
- Magee, C., Jackson, C. A. L., and Schofield, N. (2013). The influence of normal fault geometry on igneous sill emplacement and morphology. *Geology* 41, 407–410. doi: 10.1130/G33824.1
- Makhankova, A., Sautter, B., Mathew, M., Menier, D., and Poppelreiter, M. (2020). Seismic stratigraphy and sedimentology of a Miocene carbonate platform in Luconia, South China Sea. *Geological J.* 56, 1–17. doi: 10.1002/gj.3942
- Mohn, G., Manatschal, G., Beltrando, M., Masini, E., and Kuszniir, N. (2012). Necking of continental crust in magma-poor rifted margins: Evidence from the fossil Alpine Tethys margins. *Tectonics* 2012, 31(1). doi: 10.1016/j.jvolgeores.2017.07.022
- Montanari, D., Bonini, M., Corti, G., Agostini, A., and Ventisette, D. C. (2017). Forced folding above shallow magma intrusions: Insights on supercritical fluid flow from analogue modelling. *J. Volcanol. Geothermal Res.* 345, 67–80. doi: 10.1016/j.jvolgeores.2017.07.022

- Pang, X., Ren, J., Zheng, J., Liu, J., Yu, P., and Liu, B. (2018). Petroleum geology controlled by extensive detachment thinning of continental margin crust: A case study of Baiyun sag in the deep-water area of northern South China Sea. *Petroleum Explor. Dev.* 45, 29–42. doi: 10.1016/S1876-3804(18)30003-X
- Pinglu, L., and Chuntao, R. (1994). Tectonic characteristics and evolution history of the Pearl river mouth basin. *Geol. Geophys. South China Sea Env.* 235, 13–25. doi: 10.1016/0040-1951(94)90014-0
- Planke, S., Rasmussen, T., Rey, S. S., and Myklebust, R. (2005). “Seismic characteristics and distribution of volcanic intrusions and hydrothermal vent complexes in the Vøring and Møre basins,” in *Geological Society, London, Petroleum Geology Conference Series*, Vol. 6. 833–844 (The Geological Society of London). doi: 10.1144/0060833
- Pomar, L., Bassant, P., Brandano, M., Ruchonnet, C., and Janson, X. (2012). Impact of carbonate producing biota on platform architecture: insights from Miocene examples of the Mediterranean region. *Earth-Science Rev.* 113, 186–211. doi: 10.1016/j.earscirev.2012.03.007
- Pomar, L., and Kendall, C. G. S. C. (2008). A Response to Hydrodynamics and Evolving Ecology”, Controls on Carbonate Platform and Reef Development, Jeff Lukasik, J.A. (Toni) Simo 2008. doi: 10.2110/pec.08.89.0187
- Prat, S., Jorry, S. J., Jouet, G., Camoin, G., Vella, C., Roy, L. P., et al. (2016). Geomorphology and sedimentology of a modern isolated carbonate platform: The Glorieuses archipelago, SW Indian Ocean. *Mar. Geol.* 380, 272–283. doi: 10.1016/j.margeo.2016.04.009
- Qiao, J., Luan, X., Raveendrasinghe, T. D., Lu, Y., Fan, G., Wei, X., et al. (2024). Unravelling Cenozoic carbonate platform fluid expulsion: Deciphering pockmark morphologies and genesis in the Tanintharyi shelf of the Andaman Sea as promising hydrocarbon reservoirs. *Mar. Petroleum Geol.* 160, 106603. doi: 10.1016/j.marpetgeo.2023.106603
- Ren, J., Pang, X., Lei, C., Yuan, L., Liu, J., and Yang, L. (2015). Ocean and continent transition in passive continental margins and analysis of lithospheric extension and breakup process: Implication for research of the deepwater basins in the continental margins of South China Sea. *Earth Sci. Front.* 22, 102.
- Reolid, J., Betzler, C., Braga, J. C., Lüdmann, T., Ling, A., and Eberli, G. P. (2020). Facies and geometry of drowning steps in a Miocene carbonate platform (Maldives). *Palaeogeogr. Palaeoclimatol. Palaeoecol.* 538, 109455. doi: 10.1016/j.palaeo.2019.109455
- Riding, R. (2002). Structure and composition of organic reefs and carbonate mud mounds: concepts and categories. *Earth-Science Rev.* 58, 163–231. doi: 10.1016/S0012-8252(01)00089-7
- Shahzad, K., Betzler, C., Ahmed, N., Ahmed, N., Qayyum, F., Spezzaferri, S., et al. (2018). Growth and demise of a Paleogene isolated carbonate platform of the Offshore Indus Basin, Pakistan: effects of regional and local controlling factors. *Int. J. Earth Sci.* 107, 481–504. doi: 10.1007/s00531-017-1504-7
- Shao, L., Cui, Y., Qiao, P., Zhang, D., Liu, X., and Zhang, C. (2017). Sea-level changes and carbonate platform evolution of the Xisha Islands (South China Sea) since the Early Miocene. *Palaeogeogr. Palaeoclimatol. Palaeoecol.* 485, 504–516. doi: 10.1016/j.palaeo.2017.07.006
- Silva, R. O., Leite, M. G. P., Krahl, G., Rudnitzki, I., Santos, S. I. A., Souza, M. L., et al. (2024). Neogene isolated carbonate platform of the Rio Grande rise (southwest Atlantic ocean). *J. South Am. Earth Sci.* 145, 105044. doi: 10.1016/j.jsames.2024.105044
- Su, X., Xiang, R., Yi, L., Zhang, Y., Qin, G., and Yan, W. (2024). Neogene carbonate platform development in the southern South China Sea: Evidence from calcareous microfossils. *Palaeogeogr. Palaeoclimatol. Palaeoecol.* 640, 112093. doi: 10.1016/j.palaeo.2024.112093
- Sun, Q., Wu, S., Cartwright, J., Wang, S., Lu, Y., Chen, D., et al. (2014). Neogene igneous intrusions in the northern South China Sea: Evidence from high-resolution three dimensional seismic data. *Mar. Petroleum Geol.* 54, 83–95. doi: 10.1016/j.marpetgeo.2014.02.014
- Sun, Z., Xu, Z., Sun, L., Pang, X., Yan, C., Li, Y., et al. (2014). The mechanism of post-rift fault activities in Baiyun sag, Pearl River Mouth basin. *J. Asian Earth Sci.* 89, 76–87. doi: 10.1016/j.jseas.2014.02.018
- Svensen, H., Planke, S., Malthe-Sørensen, A., Jamtveit, B., Myklebust, R., Rasmussen Eidem, T., et al. (2004). Release of methane from a volcanic basin as a mechanism for initial Eocene global warming. *Nature* 429, 542–545. doi: 10.1038/nature02566
- Tang, X., Cryton, P., Gao, Y., Huang, Y., and Bian, W. (2015). Types and characteristics of volcanostratigraphic boundaries and their oil-gas reservoir significance. *Acta Geologica Sinica-English Edition* 89, 163–174. doi: 10.1111/1755-6724.12402
- Tian, D., Jiang, T., Liu, B., Liu, J., Zhang, Z., Xu, H., et al. (2019). Early Miocene sedimentary processes and their hydrocarbon implications in the Baiyun Sag of Pearl River Mouth Basin, northern South China sea. *Mar. Petroleum Geol.* 101, 132–147. doi: 10.1016/j.marpetgeo.2018.11.044
- Tian, J., Wu, S., Lv, F., Wang, D., Wang, B., Zhang, X., et al. (2015). Middle Miocene mound-shaped sediment packages on the slope of the Xisha carbonate platforms, South China Sea: Combined result of gravity flow and bottom current. *South China Sea Deep* 122, 172–184. doi: 10.1016/j.dsr.2.2015.06.016
- Ting, K., Tan, Y., Chiew, E., Lee, L., Azudin, A. N., and Ishak, N. A. (2021). “Assessing controls on isolated carbonate platform development in Central Luconia, NW Borneo, from a regional 3D seismic facies and geomorphology investigation,” in *Seismic Characterization of Carbonate Platforms and Reservoirs*. Eds. J. Hendry, P. Burgess, D. Hunt, X. Janson and V. Zampetti (London, UK: Geological Society of London), 0. doi: 10.1144/SP509-2019-89
- Tomás, S., Löser, H., and Salas, R. (2008). Low-light and nutrient-rich coral assemblages in an Upper Aptian carbonate platform of the southern Maestrat Basin (Iberian Chain, eastern Spain). *Cretac. Res.* 29, 509–534. doi: 10.1016/j.cretres.2007.09.001
- Tucker, M. E., Carey, S. N., Sparks, R. S. J., Stinton, A., Leng, M., Robinson, L., et al. (2020). Carbonate crusts around volcanic islands: Composition, origin and their significance in slope stability. *Mar. Geol.* 429, 106320. doi: 10.1016/j.margeo.2020.106320
- Van Wagoner, J. C., Posamentier, H. W., Mitchum, R. M., Vail, P. R., Sarg, J. F., Loutit, T. S., et al. (1988). “An overview of the fundamentals of sequence stratigraphy and key definitions,” in *Sea-Level Changes: an Integrated Approach*, vol. 42. Eds. C. K. Wilgus, B. S. Hastings, C. G. St. C. Kendall, H. W. Posamentier, C. A. Ross and J. C. Van Wagoner (Tulsa, OK, USA: Society of Economic Paleontologists and Mineralogists Special Publication), 39–45. doi: 10.2110/pec.88.01.0039
- Wright, I. C. (2001). *In situ* modification of modern submarine hyaloclastic/pyroclastic deposits by oceanic currents: an example from the Southern Kermadec arc (SW Pacific). *Mar. Geol.* 172, 287–307. doi: 10.1016/S0025-3227(00)00131-6
- Wu, F., Xie, X., Zhu, Y., Coletti, G., Betzler, C., Cui, Y., et al. (2021). Early development of carbonate platform (Xisha Islands) in the northern South China Sea. *Mar. Geol.* 441, 106629. doi: 10.1016/j.margeo.2021.106629
- Wu, S., Yang, Z., Wang, D., Lv, F., Lüdmann, T., Fulthorpe, C., et al. (2014). Architecture, development and geological control of the Xisha carbonate platforms, northwestern South China Sea. *Mar. Geol.* 350, 71–83. doi: 10.1016/j.margeo.2013.12.016
- Yan, P., Deng, H., Liu, H., Zhang, Z., and Jiang, Y. (2006). The temporal and spatial distribution of volcanism in the South China Sea region. *J. Asian Earth Sci.* 27, 647–659. doi: 10.1016/j.jseas.2005.06.005
- Zeng, Z., Zhu, H., Yang, X., Zhang, G., and Zeng, H. (2019). Three-dimensional imaging of Miocene volcanic effusive and conduit facies: Implications for the magmatism and seafloor spreading of the South China Sea. *Mar. Pet. Geol.* 109, 193–207. doi: 10.1016/j.marpetgeo.2019.06.024
- Zhang, M., Lin, C., He, M., Zhang, Z., Li, H., Feng, X., et al. (2019). Stratigraphic architecture, shelf-edge delta and constraints on the development of the Late Oligocene to Early Miocene continental margin prism, the Pearl River Mouth Basin, northern South China Sea. *Mar. Geol.* 416, 105982. doi: 10.1016/j.margeo.2019.105982
- Zhang, Y., Yu, K., and Li, S. (2024). U-Pb zircon geochronology of basaltic pyroclastic rocks from the basement beneath the Xisha Islands in the northwestern South China Sea and its geological significance. *Acta Oceanologica Sin.*, 1–11. doi: 10.1007/s13131-023-2198-2
- Zhao, F., Alves, T. M., Wu, S., Li, W., Huuse, M., and Mi, L. (2016). Prolonged post-rift magmatism on highly extended crust of divergent continental margins (Baiyun Sag, South China Sea). *Earth Planetary Sci. Lett.* 445, 79–91. doi: 10.1016/j.epsl.2016.04.001
- Zhou, D., Sun, Z., Liao, J., Zhao, Z., He, M., Wu, X., et al. (2009). Filling history and post-breakup acceleration of sedimentation in baiyun sag, deepwater Northern South China sea. *J. Earth Sci.* 20, 160–171. doi: 10.1007/s12583-009-0015-2
- Zhou, W., Zhuo, H., Wang, Y., Xu, Q., and Li, D. (2020). Post-rift submarine volcanic complexes and fault activities in the Baiyun Sag, Pearl River Mouth Basin: New insights into the breakup sequence of the northern South China Sea. *Mar. Geol.* 430, 106338. doi: 10.1016/j.margeo.2020.106338